

Supporting Information on: Noncontact Viscoelastic Measurement of Polymer Thin Films in a Liquid Medium Using Long-Needle Atomic Force Microscopy

Dongshi Guan[†], Chloé Barraud[‡], Elisabeth Charlaix[‡], and Penger Tong^{†,*}

[†]*Department of Physics, Hong Kong University of Science and Technology, Clear Water Bay, Kowloon, Hong Kong and*

[‡]*LIPHY, Université Grenoble Alpes, F-38000 Grenoble, France*

CONTENTS

I. Fabrication of long needle probe	1
II. Measurement of power spectrum of the long needle probe	1
III. Calibration of the driving force	2
IV. Determination of contact point	3
V. Measured damping coefficient and added mass of long needle probe	4
VI. Numerical calculation of the correction function $\tilde{p}^*(D/D_c)$	4
References	5

I. FABRICATION OF LONG NEEDLE PROBE

The fabrication of the long needle probe contains two major parts: (i) connecting a glass fiber to the front end of a AFM cantilever and (ii) forging the fiber tip to be sharp and spherical. The assembly of the glass fiber probe is carried out under a high-magnification stereomicroscope (Leica MZ16) using a motorized micro-manipulator system. The thin glass fiber is pulled out of a glass rod of diameter 1.0 mm using a programmed pippette puller (P-97, Sutter Instrument). A homemade tweezer is made to cut off the thin tip of the tapered fiber with a desired diameter (0.5-5 μm). Commercial gold coated silicon nitride cantilevers (BL-TR800PB, Asylum) are used in the experiment. An UV-curable glue (Norland, NOA 81) is used to permanently connect the glass fiber to the front end of the cantilever beam. The fiber has a tilt angle of 11° with respect to the cantilever normal, so that the hanging fiber becomes normal to the liquid-air interface when the cantilever is mounted to the AFM holder. The aligned fiber with a desired diameter is then inserted into the middle of a semi-spherical glue drop on the cantilever beam and cured under radiation of a UV light (Lightning Enterprises, ELC-410) for 15 minutes. The glass fiber is then cut with a desired length, typically 100 – 300 μm .

After the assembly of the fiber probe, the tip of the glass fiber is further forged to a desired shape using a micro-forge (MF-900, Narishige). The heater of the micro-forge is used first to melt a glass bead, which is used as a glass bath. The temperature of the heater is adjusted to be slightly higher than the melting temperature of the glass, and the fiber tip is then brought into contact with the glass bath to melt the tip by heating. Here the adjustment of the temperature should be fast and precise so that it is high enough to just melt the fiber tip but not to soften and bend the long fiber. The fiber is then pulled out of the glass bath and a spike will form at the tip if the temperature is just right. Finally, the spike is kept close to the hot glass bath so that it can be gradually melt and annealed. In this way, the fiber tip is forged to be sharp and spherical, as shown in Fig. 1(b) of the main text. Typically, the tip radius R can be controlled in the range 50-1000 nm using different temperatures and annealing times.

After the fabrication, the freshly made needle probe is cleaned using a low vacuum plasma cleaner at the power 40W for 15 minutes. The vacuum chamber is kept at ~ 600 milli-torr during the plasma cleaning. The freshly cleaned fiber probe is hydrophilic with a contact angle ~ 0 degree at the water-air and decane-air interfaces without hysteresis. The wetting properties of the fiber can be examined using the same AFM setup [1].

II. MEASUREMENT OF POWER SPECTRUM OF THE LONG NEEDLE PROBE

When the needle probe is positioned stationary at the liquid-air interface far from the lower surface, the vertical displacement $z(t)$ of the needle (\equiv vertical deflection of the AFM cantilever) is well described by the Langevin equation [2, 3]

$$m\ddot{z} + \xi\dot{z} + k_c z = f_B(t), \quad (\text{S1})$$

where $f_B(t)$ is the random Brownian force due to thermal fluctuations of the surrounding fluid. While the mean value of $f_B(t)$ is zero, its autocorrelation function has a form [4] $C(\tau) = \langle f_B(t + \tau)f_B(t) \rangle = 2k_B T \xi \delta(\tau)$, where $k_B T$ is the thermal energy of the system and $\delta(\tau)$ is the δ function. The power spectrum density (PSD), $|z(\tilde{\omega})|^2$, of vertical deflections of the cantilever can be solved analytically from Eq. (S1) [5, 6],

$$|z(\tilde{\omega})|^2 = \frac{2k_B T \xi / m^2}{(\omega_0^2 - \tilde{\omega}^2)^2 + (\tilde{\omega} \xi / m)^2}, \quad (\text{S2})$$

* Corresponding email address: pengert@ust.hk

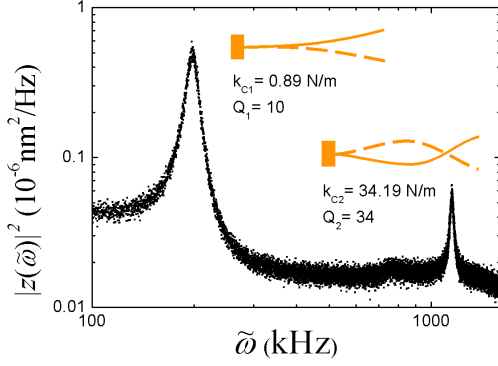


FIG. S1. Measured $|z(\tilde{\omega})|^2$ as a function of $\tilde{\omega}$ for the modified cantilever. The measurement is made when the glass needle is partially immersed through the decane-air interface with immersion length $h = 30 \mu\text{m}$. The inset shows the bending modes of the cantilever at the first two resonances and the corresponding values of the spring constant k_c and quality factor Q .

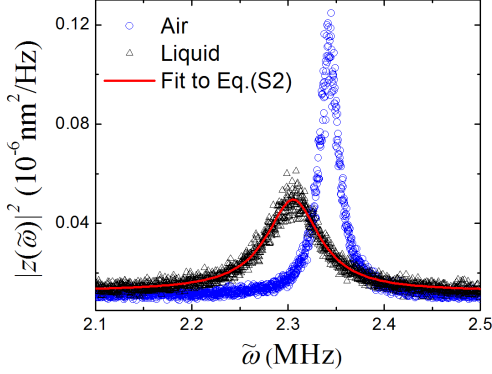


FIG. S2. Measured $|z(\tilde{\omega})|^2$ for the modified cantilever with the long glass needle in air (blue circles) and in decane with immersion length $h = 30 \mu\text{m}$ (black triangles). Only the second resonant peak is shown in the plot. The red solid line is a fit to Eq. (S2) to the black triangles with $m = 6.43 \times 10^{-9}$ g, $\xi = 4.38 \times 10^{-7}$ Nm/s, and $\omega_0 = 2.30579$ MHz.

where $\tilde{\omega} = 2\pi f$ is the angular frequency arriving from the Fourier transform of the measured time-varying cantilever signal and $\omega_0 = (k_c/m)^{1/2}$ is the mechanical resonant frequency of the cantilever system.

Figure S1 shows measured $|z(\tilde{\omega})|^2$ as a function of $\tilde{\omega}$ for the modified cantilever. The measurement is made when the glass needle is partially immersed through the decane-air interface with immersion length $h = 30 \mu\text{m}$. The two resonant peaks correspond to the first two normal bending modes of the modified cantilever, as illustrated in the inset of Fig. S1. Equation (S2) is used to fit the data for each peak, from which one obtains the spring constant k_c and quality factor Q of each mode [7]. The fitting results are listed in the inset of Fig. S1. It is found that the quality factor Q_2 of the second bending mode is improved significantly. Because the accuracy of

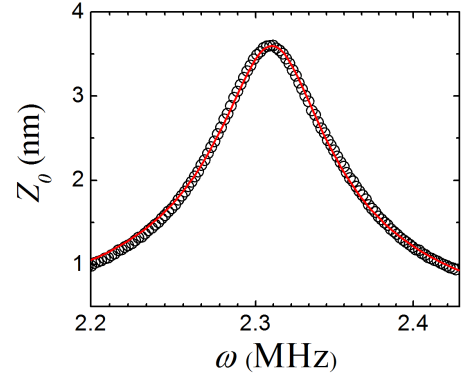


FIG. S3. Measured oscillation amplitude Z_0 (black circles) as a function of driving frequency ω for the modified cantilever under a constant driving force F_0 . The measurement is made when the glass needle is partially immersed through the decane-air interface with $h = 30 \mu\text{m}$, and the applied ac voltage to the cantilever holder is kept at a constant amplitude $V_0 = 0.2$ V. The red solid line is a fit of Eq. (2) of the main text to the data points with $F_0 = 0.59$ nN, $\xi = 4.13 \times 10^{-7}$ Nm/s, and $\omega_0 = 2.31057$ MHz.

the resonant frequency locking in the FM mode is determined by the Q -factor [8, 9], we use the second resonance mode for the FM-AFM in the liquid medium.

Figure S2 shows a magnified plot of the second resonant peak for the modified cantilever with the long glass needle in air (blue circles) and in decane with $h = 30 \mu\text{m}$ (black triangles). The measured $|z(\tilde{\omega})|^2$ in decane is well described by Eq. (S2) (red solid line). It is seen that the resonant peak in decane is only shifted by 2% compared with that in air, indicating that the effects of the added mass and viscous damping to the long needle are relatively small. With the fitted values of m , ξ , and ω_0 , we obtain the spring constant $k_c = m\omega_0^2 = 34.19$ N/m and quality factor $Q = \omega_0 m / \xi = 34$ in decane. The frequency resolution of the FM-AFM mode is given by [8, 9]

$$\omega_{min} = \sqrt{\frac{2k_B T \omega_0 \Delta B}{k_c Q Z_0^2}}, \quad (\text{S3})$$

where $\Delta B \simeq 1.5$ kHz is a typical value of the bandwidth set by the FM-AFM, and the oscillation amplitude $Z_0 \simeq 2$ nm. From Eq. (S3) we find $\omega_{min} \simeq 78$ Hz for our setup, which is sufficient to resolve the large variations of the measured ω'_0 , as shown in Fig. 2(b) of the main text.

III. CALIBRATION OF THE DRIVING FORCE

In the experiment, the long needle probe is mounted on the cantilever holder with an electromagnetic actuator (iDrive, Asylum Research), which has a better frequency response than the conventional piezo-electric actuator for the dynamic mode AFM. Figure S3 shows the measured oscillation amplitude Z_0 as a function of driving frequency ω for the modified cantilever under a constant

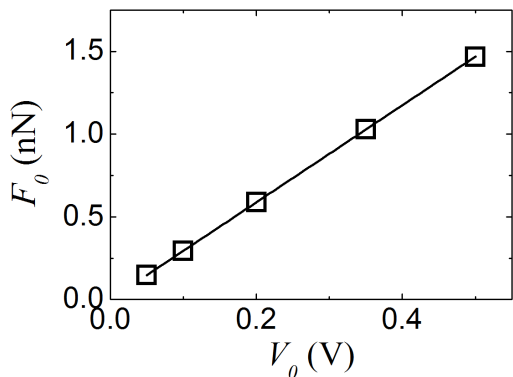


FIG. S4. Fitted values of the driving force F_0 as a function of the applied voltage V_0 . The solid line is a linear fit to the data points.

driving force F_0 . The measurement is made when the glass needle is partially immersed through the decane-air interface with immersion length $h = 30 \mu\text{m}$, and the applied AC voltage to the cantilever holder is kept at a constant amplitude $V_0 = 0.2 \text{ V}$. The red solid line is a fit of Eq. (2) of the main text (with $K^*(D) = 0$) to the data points with three fitting parameters: the amplitude of the driving force F_0 , the damping coefficient ξ , and the resonant frequency ω_0 . The effective mass m is already obtained from the measured PSD, as shown in Fig. S2. It is seen that the data are well described by Eq. (2) of the main text and the fitted values of $\xi = 4.1310 \times 10^{-7} \text{ Nm/s}$ and $\omega_0 = 2.31057 \text{ MHz}$ agree well with those obtained from the measured PSD, as shown in Fig. S2. From the resonance curve as shown in Fig. S3, we obtain the value of $F_0 = 0.59 \text{ nN}$ for a given applied voltage $V_0 = 0.2 \text{ V}$.

Figure S4 shows the calibration curve $F_0(V_0)$ as a function of the applied voltage V_0 . The data are well described by a linear function $F_0 = a + bV_0$ with $a = 0.95 \text{ pN}$ and $b = 2.93 \text{ nN/V}$ (solid line). With the calibrated curve $F_0(V_0)$, one can control the driving force F_0 at the accuracy of nano-Newtons by varying the applied voltage V_0 .

IV. DETERMINATION OF CONTACT POINT

In the experiment, we use two separate methods to determine the contact point between the needle tip and PDMS film. The first method is to directly measure the deflection z of the cantilever as the needle tip slowly moves toward the lower PDMS surface at a constant speed u . Figure S5(a) shows the measured z as a function of surface separation D' between the needle tip and PDMS film. When the needle tip touches the PDMS surface, the hard-wall repulsion forces the cantilever to reverse its bending direction and the deflection z reveals a sharp linear rise as the z -axis piezo goes down further. This sharp upturn point is used to define the contact point $D' = 0$. For $D' > 0$, the measured deflection z

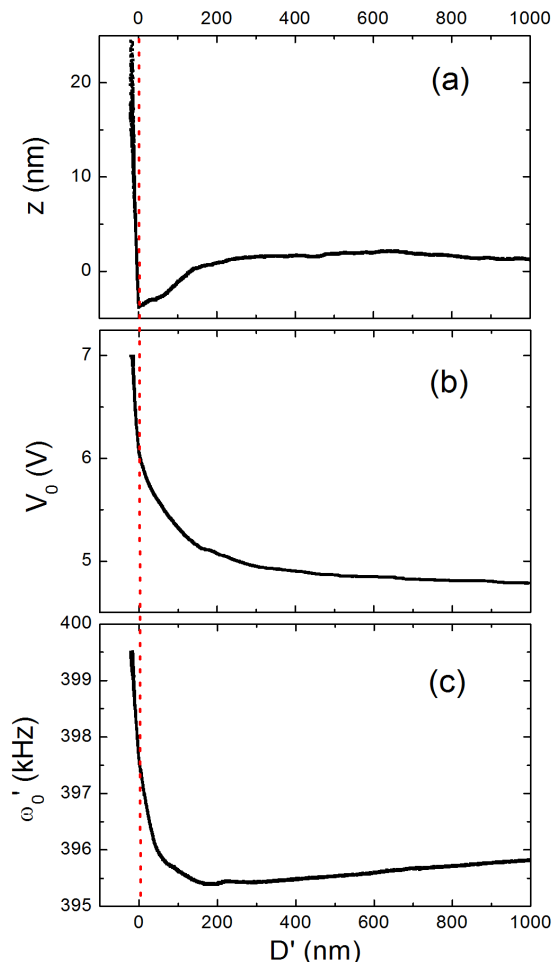


FIG. S5. Simultaneously measured deflection z , driving voltage V_0 , and resonant frequency ω'_0 of the AFM cantilever as a function of surface separation D' between the needle tip and PDMS film. The measurement is made with the needle tip approaching the PDMS surface at a constant speed $u = 100 \text{ nm/s}$. The red vertical dotted line indicates the contact point $D' = 0$.

shows some fluctuations around zero, which are caused by the stick-slip motion (pinning and depinning) of the moving contact line between the liquid interface and needle surface.

During the steady-state DC measurement of deflection z , the cantilever is also frequency modulated at its resonance with a small amplitude Z_0 ($\sim 2 \text{ nm}$), from which we simultaneously measure the driving voltage V_0 and resonant frequency ω'_0 as a function of D' . Figure S5(b) and S5(c) show, respectively, how the measured V_0 and ω'_0 rapidly increase with the needle tip approaching the PDMS surface. As discussed above, V_0 is linked to the driving force F_0 , which is related to the dissipation $\xi' = F_0/Z_0\omega'_0$ at resonance. To avoid direct contact and damaging the PDMS surface by the hard press of the needle tip, the cantilever is set to automatically retreat from the PDMS surface once V_0 reaches a chosen set-

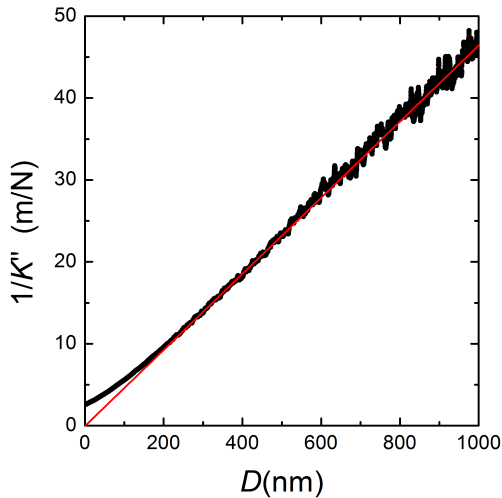


FIG. S6. Measured $1/K''(D)$ as a function of tip-sample distance D . The red solid line is a linear fit to the data points at large values of D with $D > 200$ nm.

point value, such as 5.9 V as shown in Fig. S5(b).

The second method to determine the contact point is to take extrapolation of the measured $1/K''(D)$ at large values of tip-sample distance D to the limit of small D , as shown in Fig. S6. For $D > D_c$, the Reynolds damping force is given by [10, 11], $1/K''(D) = D/(6\pi\eta_0\omega_0^2 R^2)$, which is a linear function of D and fits the data at large D very well (red solid line). By extrapolating this linear function to the limit of infinite dissipation ($1/K''(D) = 0$), we find the contact point $D = 0$. The experimental uncertainty in determining the actual contact point is typically $\delta D = |D' - D| \simeq \pm 5$ nm, which is small compared with the cut-off distance $D_c (\simeq 90$ nm), below which the measured response functions, $K'(D)$ and $K''(D)$, saturate at a contact value, as shown in Figs. 3 and 4 of the main text. In the data analysis presented in the main text, we use the second method to determine the contact point ($D = 0$).

V. MEASURED DAMPING COEFFICIENT AND ADDED MASS OF LONG NEEDLE PROBE

When the glass fiber is in contact with a liquid interface, the resonant peak broadens while the peak height decreases and peak position shifts toward a lower frequency. These changes continue when the immersion length h of the fiber increases [3]. This is caused by the increasing viscous damping ξ and added mass Δm resulting from a thin layer of fluid in the vicinity of the fiber surface, which oscillates with the fiber probe. For a long cylindrical fiber of diameter d partially immersed in an infinite liquid of viscosity η_0 , its friction coefficient ξ parallel to the long axis of the cylinder takes the form

[6, 12]

$$\xi \simeq \alpha \pi d \eta_0 + \frac{2\pi\eta_0 h}{\ln(h/d) + \varepsilon} + \frac{1}{2} \pi d h \sqrt{2\eta_0 \rho \omega}, \quad (\text{S4})$$

where the first term is the contribution from the contact line between the fiber surface and liquid-air interface with $\alpha = 1.1 \pm 0.3$. The second term is the zero-frequency contribution from the bulk liquid, where h is the fiber immersion length in the liquid and $\varepsilon \simeq -0.55$ is a correction factor for the cylinder with $h/d > 4$ [13]. The last term is the frequency-dependent contribution from the bulk liquid, where ρ is the fluid density and ω is the oscillation frequency. For large values of h , the friction coefficient ξ is approximately a linear function of h (i.e., $\xi \simeq a + bh$), as $\ln(h/d)$ does not change much with h and the last term dominates in our working frequency range.

For a liquid film of thickness h_0 above the PDMS surface, the fiber immersion length can be written as $h = h_0 - D$, where D is the tip-sample distance. Therefore, we have

$$\xi(D) \simeq a + b(h_0 - D) = (a + bh_0) - bD = a' - bD, \quad (\text{S5})$$

which is used to fit the data, as shown by the red line in Fig. 2(a) of the main text.

The added mass Δm is given by [14]

$$\Delta m = \pi(d/2)^2 h \rho + \frac{1}{2} \pi d h \sqrt{2\eta_0 \rho / \omega}, \quad (\text{S6})$$

where the first term represents the mass of the displaced fluid. The second term is the frequency-dependent contribution resulting from a thin layer of fluid of thickness $\delta \simeq (2\eta_0/\rho\omega)^{1/2}$ oscillating with the fiber. The added mass Δm is proportional to the fiber immersion length, $h = h_0 - D$, and thus changes the resonant frequency from $\omega_0 = (k_c/m_0)^{1/2}$ (in air) to,

$$\omega_0(D) = \left(\frac{k_c}{m_0 + \Delta m(D)} \right)^{1/2} \simeq \frac{\omega_0}{(c - eD)^{1/2}}, \quad (\text{S7})$$

where c and e are two fitting parameters which depend on the fiber diameter d and liquid film thickness h_0 . Equation (S7) is used to fit the data, as shown by the green line in Fig. 2(b) of the main text.

VI. NUMERICAL CALCULATION OF THE CORRECTION FUNCTION $\tilde{p}^*(D/D_c)$

The linear response theory of the elasto-hydrodynamics (EHD) under the sphere-plane geometry, which has been described in Ref. [11], predicted that the complex response function $K^*(D) \equiv K'(D) + iK''(D)$ has a scaling form

$$K^*(D) = i \frac{6\pi\eta_0\omega R^2}{D} \tilde{p}^* \left(\frac{D}{D_c} \right), \quad (\text{S8})$$

where R is the radius of the fiber tip, ω is the driving angular frequency, and D is the tip-sample distance. The correction function $\tilde{p}^*(D/D_c)$, which describes the film compliance, is obtained from the solution of the integral equation [11]

$$\tilde{p}^*(\zeta) = \zeta K_1(\zeta) - 3i \left(\frac{D_c}{D} \right)^{3/2} \int_0^\infty d\zeta' \tilde{p}^*(\zeta') X(\zeta' \tau') M(\zeta, \zeta'), \quad (\text{S9})$$

where $\tau' = \tau/(2RD)^{1/2}$ is the reduced film thickness,

$$D_c = 8R \left[\frac{(1-\nu^2)\eta_0\omega}{E} \right]^{2/3} \quad (\text{S10})$$

is a cut-off distance with E being the Young's modulus and ν the Poisson ratio of the film, and the kernel $M(\zeta, \zeta')$ is an integral function

$$M(\zeta, \zeta') = \int_0^\infty dx \frac{x J_1(\zeta x) J_1(\zeta' x)}{\zeta \zeta' (1+x^3)^2}. \quad (\text{S11})$$

Here $M(\zeta, \zeta')$ satisfies the conditions $M(\zeta, \zeta') = M(\zeta', \zeta)$ and

$$M(\zeta < \zeta') = \frac{\zeta^2 + \zeta'^2}{8\zeta\zeta'} I_1(\zeta) K_1(\zeta') - \frac{I_2(\zeta) K_2(\zeta')}{4}, \quad (\text{S12})$$

where J_1 is the first order Bessel function and I_n and K_n are the n th order modified Bessel functions. Finally, the function $X(\zeta\tau')$ in Eq. (S9) describes the film response to an axial symmetric pressure field and is given by [15]

$$X(\zeta\tau') = \frac{1 + 4be^{-2\zeta\tau'} - abe^{-4\zeta\tau'}}{1 - [a + b + 4b(\zeta\tau')^2]e^{-2\zeta\tau'} + abe^{-4\zeta\tau'}}, \quad (\text{S13})$$

where

$$a = \frac{\beta\gamma - \gamma_s}{\beta\gamma + 1}, \quad b = \frac{\beta - 1}{\beta + \gamma_s}, \quad \beta = \frac{G}{G_s}, \quad \gamma_i = 3 - 4\nu_i.$$

In the above, $G = E/2(1 + \nu)$ is the shear modulus of the film and $G_s = E_s/2(1 + \nu_s)$ is that of the substrate.

In the original model of EHD [11], the film under study was assumed to be purely elastic and thus only the elastic deformation of the film was considered. It is quite straightforward to include the viscoelasticity effect

of the film by introducing a complex Young's modulus $E^* = E + iE''$ in Eqs. (S10) and (S13). In this case, we keep the Poisson ratio $\nu = 1/2$, and therefore we have $E^* = 2(1 + \nu)G^* = 3G^*$ (with $G^* = G + iG''$).

For each value of D , the integral equation (S9) can be discretized into the following linear matrix equation for a finite number of values ζ_i with $i = 1, 2, \dots, N$:

$$\mathbf{p} = \mathbf{b} - 3i\lambda\bar{\mathbf{K}}\mathbf{p}, \quad (\text{S14})$$

where \mathbf{p} is a vector with the component $p_i = \tilde{p}^*(\zeta_i)$ and λ is the complex value of $(D_c/D)^{3/2}$. The vector \mathbf{b} is given by $b_i = \zeta_i K_1(\zeta_i)$ and the matrix $\bar{\mathbf{K}}$ takes the form $K_{ij} = M(\zeta_i, \zeta_j) X(\zeta_j \tau') w_j$ with w_j being the Gauss-Legendre weight factor associated with ζ_j . Equation (S14) can be solved by the matrix inversion routine in the Igor Pro software. In practice, we find that it is adequate to calculate Eq. (S14) over an interval of $\zeta_i \in [0, 20]$, with a number of discretization $N = 20$.

When $D < D_c$, however, the direct inversion of the matrix $\bar{\mathbf{I}} + 3i\lambda\bar{\mathbf{K}}$ in Eq. (S14) may become quite inaccurate, giving rise to oscillations in the calculated correction function. We fix this instability problem by isolating the diagonal matrix $\bar{\mathbf{A}}$ from $\bar{\mathbf{K}}$, that is

$$\bar{\mathbf{K}} = \bar{\mathbf{A}} + \bar{\mathbf{K}}', \quad (\text{S15})$$

with $\bar{\mathbf{A}} = \text{diag}(\bar{\mathbf{K}})$, and obtain \mathbf{p} by solving the equation

$$\mathbf{p} = (\bar{\mathbf{I}} + 3i\lambda\bar{\mathbf{A}})^{-1}\mathbf{b} - 3i\lambda(\bar{\mathbf{I}} + 3i\lambda\bar{\mathbf{A}})^{-1}\bar{\mathbf{K}}'\mathbf{p}. \quad (\text{S16})$$

Once Eq. (S16) is solved, we obtain the final correction factor $\tilde{p}^*(D/D_c) = \tilde{p}^*(\zeta = 0)$ [11]. Given the system parameters $\eta, \omega, R, \tau, E, E/E'', E_s, \nu$, and ν_s , one can numerically calculate the response function $K^*(D)$ for each value of D , with $K'(D)$ and $K''(D)$ being, respectively, its real and imaginary parts, which are used to fit the experimental data. In the fitting, the Young's modulus E and viscoelastic ratio E/E'' are used as two free adjustable parameters to best fit the data.

The above numerical calculation of $\tilde{p}^*(D/D_c)$ is conducted using the Igor Pro software. Readers who are interested in the detailed numerical procedures may contact us (dsguan@connect.ust.hk) to have access to our Igor Pro code for their own applications.

-
- [1] Guan, D.; Wang, Y. J.; Charlaix, E.; Tong, P. Asymmetric and speed-dependent capillary force hysteresis and relaxation of a suddenly stopped moving contact line. *Phys. Rev. Lett.* **2016**, *116*, 066102.
- [2] Ma, H.; Jimenez, J.; Rajagopalan, R. Brownian fluctuation spectroscopy using atomic force microscopes *Langmuir* **2000**, *16*, 2254-2261.
- [3] Xiong, X.; Guo, S.; Xu, Z.; Sheng, P.; Tong, P. Development of an atomic-force-microscope-based hanging-fiber rheometer for interfacial microrheology. *Phys. Rev. E* **2009**, *80*, 061604.
- [4] Reif, F. *Fundamentals of Statistical and Thermal Physics*; McGraw-Hill, 1985.
- [5] Benmouna, F.; Johannsmann, D. Hydrodynamic interaction of AFM cantilevers with solid walls: An investigation based on AFM noise analysis. *Eur. Phys. J. E* **2002**, *9*, 435-441.
- [6] Guo, S.; Gao, M.; Xiong, X.; Wang, Y. J.; Wang, X.;

- Sheng, P.; Tong, P. Direct Measurement of Friction of a Fluctuating Contact Line. *Phys. Rev. Lett.* **2013**, *111*, 026101.
- [7] Guan, D.; Hang, Z. H.; Marcet, Z.; Liu, H.; Kravchenko, I. I.; Chan, C. T.; Chan, H. B.; Tong, P. Direct measurement of optical force induced by near-field plasmonic cavity using dynamic mode AFM. *Sci. Rep.* **2015**, *5*, 16216.
- [8] Fukuma, T.; Kilpatrick, J. I.; Jarvis, S. P. Phase modulation atomic force microscope with true atomic resolution. *Rev. Sci. Instrum.* **2006**, *77*, 123703.
- [9] Kobayashi, K.; Yamada, H.; Matsushige, K. Frequency noise in frequency modulation atomic force microscopy. *Rev. Sci. Instrum.* **2009**, *80*, 043708.
- [10] Brenner, H. The slow motion of a sphere through a viscous fluid towards a plane surface. *Chem. Eng. Sci.* **1961**, *16*, 242-251.
- [11] Leroy, S.; Charlaix, E. Hydrodynamic interactions for the measurement of thin film elastic properties. *J. Fluid Mech.* **2011**, *674*, 389-407.
- [12] Guo, S.; Lee, C. H.; Sheng, P.; Tong, P. Measurement of contact-line dissipation in a nanometer-thin soap film. *Phys. Rev. E* **2015**, *91*, 012404.
- [13] Devailly, C.; Laurent, J.; Steinberger, A.; Bellon, L.; Ciliberto, S. Mode coupling in a hanging-fiber AFM used as a rheological probe. *Europhys. Lett.* **2014**, *106*, 54005.
- [14] Landau, L. D.; Lifshitz, E. M. *Fluid Mechanics (2nd ed.)*; Butterworth-Heinemann, 1986.
- [15] Li, J.; Chou, T.-W. Elastic field of a thin-film/substrate system under an axisymmetric loading. *Int. J. Solids Struct.* **1997**, *34*, 4463-4478.